

# High power diode laser surface hardening of AISI 4130; statistical modelling and optimization

Moradi, M. & KaramiMoghadam, M.

Author post-print (accepted) deposited by Coventry University's Repository

**Original citation & hyperlink:**

Moradi, M & KaramiMoghadam, M 2019, 'High power diode laser surface hardening of AISI 4130; statistical modelling and optimization', *Optics and Laser Technology*, vol. 111, pp. 554-570.

<https://dx.doi.org/10.1016/j.optlastec.2018.10.043>

DOI 10.1016/j.optlastec.2018.10.043

ISSN 0030-3992

Publisher: Elsevier

**NOTICE: this is the author's version of a work that was accepted for publication in *Optics and Laser Technology*. Changes resulting from the publishing process, such as peer review, editing, corrections, structural formatting, and other quality control mechanisms may not be reflected in this document. Changes may have been made to this work since it was submitted for publication. A definitive version was subsequently published in *Optics and Laser Technology*, 111, (2019) DOI: 10.1016/j.optlastec.2018.10.043**

© 2019, Elsevier. Licensed under the Creative Commons Attribution-NonCommercial-NoDerivatives 4.0 International <http://creativecommons.org/licenses/by-nc-nd/4.0/>

Copyright © and Moral Rights are retained by the author(s) and/ or other copyright owners. A copy can be downloaded for personal non-commercial research or study, without prior permission or charge. This item cannot be reproduced or quoted extensively from without first obtaining permission in writing from the copyright holder(s). The content must not be changed in any way or sold commercially in any format or medium without the formal permission of the copyright holders.

This document is the author's post-print version, incorporating any revisions agreed during the peer-review process. Some differences between the published version and this version may remain and you are advised to consult the published version if you wish to cite from it.

# High Power Diode Laser Surface Hardening of AISI 4130; Statistical Modelling and Optimization

Mahmoud Moradi<sup>1,2</sup>, Mojtaba KaramiMoghadam<sup>1,2</sup>

<sup>1</sup> Department of Mechanical Engineering, Faculty of Engineering, Malayer University,  
Malayer, Iran

<sup>2</sup> Laser Materials Processing Research Center, Malayer University, Malayer, Iran

## Abstract:

Laser surface hardening of AISI 4130 carbon steel was conducted with a high power diode laser using Response Surface Methodology. Scanning speed, laser power and focal plane position were considered as the input process variables and cross sectional geometry of the hardened area, average micro-hardness and the ferrite phase percentage were considered as process responses. The effect of parameters on the responses variations were investigated using analysis of variance. Microstructure evaluation of the laser hardened zone was performed using optical and field emission scanning electron microscopy. Results indicated that by increasing the laser power and decreasing the scanning speed and focal plane position, higher surface hardness with more penetration in depth, higher average micro-hardness and minimum ferrite percentage will be achieved. Finally, the process was optimized by desire ability approach based on the applied statistical analyses. Minimum value of percentage of the ferrite and maximum value of the other responses are considered as optimization criteria. The recommended optimized results were validated using the experimental tests. The results show that the hardness of the diode laser hardening process is 3 times of the hardness of the base metal. Laser-overlapping scanning is performed in the optimum setting and effect of overlapping percentage is investigated.

**Keywords:** Laser Surface Hardening; Design of Experiments; High Power Diode Laser; Optimization; Overlapping.

## 1. Introduction:

Common heat treatment methods to improve the surface hardness of metals such as flame and induced heat treatment are widely used in industries. Among different laser surface treatments, laser transformation hardening (LTH) is one of the most useful and the simplest and precise methods while it does not require any accessories. High power diode laser which its applications in industry is increasing for surface engineering could be used for high accuracy surface treatment of the components. Transformation of austenite and ferrite phases to martensitic phase will improve the surface hardness by using LTH.

Laser heat treatment has been investigated since the 1970s, Hill et al. [1] used a 3 kW continuous wave CO<sub>2</sub> laser for laser surface treatment to improve the surface hardness of the tool steel (0.9% carbon and 1.7% manganese). Maximum hardened layer of 0.25 mm in depth and the maximum surface hardness of 65 HRC was obtained in their research. Benedek et al. [2] in 1980s performed laser surface hardening on four steels: AISI 1045 (carbon steel), Armco iron, AISI 4340 (alloyed steel), high speed steel M2 by using a 1.5 kW CO<sub>2</sub> CW laser. The purpose in this study is achieving higher surface hardness by varying the scanning speed and laser power without surface melting. In Armco iron some of the ferrite phases retain during the austenite transformation in laser hardening and the maximum hardness was 250 Hv in this sample. While for AISI 1045, AISI 4340 and HSS AISI M2 the maximum depth of hardness was 0.6 mm, 0.35 and 0.2 mm, respectively and the maximum hardness was around 850-900 Hv. Yang et al. [3] investigated on surface hardening of Assab DF-2 tool steel by using a 1 kW CO<sub>2</sub> laser. They have looked to find a relation between process parameters (e.g. laser power, beam diameter and scanning speed) and geometrical dimensions of hardened layer (e.g. depth and width). Their results show that the laser power and scanning speed are significant on depth of hardening. They found that the beam diameter does not affect the depth of hardness significantly while it has an important influence on the width of hardness. Surface hardening of S45C medium carbon steel has been carried out by a high power CW Nd:YAG laser by Shin et al. [4]. The uniform laser beam profile technology and the defocusing technology compared in laser hardening. The effect of the process parameters (e.g. laser power, the gas shielding pressure and the focal position) on the hardness, the hardened geometrical dimensions has been studied. They found that the hardness and the hardened area width using the designed lens are 3 times larger than those using the defocused beam. The hardened layer width and the maximum hardness were 22.3 mm and 780 Hv. Goia et al. [5] studied on surface hardening of AISI D6 tool steel by using a 2 kW Fiber laser.

Different parameters were investigated in laser hardening process by considering the laser beam energy absorptivity. The maximum hardness and depth of hardness were 800 Hv and 0.4 mm. Overlap hardening with three different overlap percentages was conducted. The hardness decreases to 480 Hv in overlapped area. Babu et al. [6] investigated the effect of Nd:YAG laser surface hardening parameters of EN25 on microstructure and hardness. Increases in surface hardness is two times the base material (370 Hv to 782 Hv). Their results show that the maximum depth of hardness is 0.7 mm and width of hardness is 2.2 mm. Adel [7] applied Nd:glass laser for laser surface hardening of Ck45 steel cylindrical rod specimens. Process parameters were considered in the experiments to improve the microstructure for better wear resistance. Martensitic microstructure with 850 Hv microhardness was obtained. In 2014 Sun et al. [8] studied on experimental and FEM numerical simulation of laser hardening of 42CrMo cast steel by a 1 kW Nd:YAG laser. A shaped beam and the Gaussian laser beam were compared in the process. They found that because of the heating rate and the high peak temperature produced by the latter shaped beam, the microhardness is higher in hardened area. A study was conducted on laser surface hardening of AISI 1045 steel by comparing the 3.5 kW High-Power Diode Laser and 15 KW CO<sub>2</sub> laser by Li et al. [9]. Numerical analysis of laser surface hardening by using two laser was investigated through FEM. The results reveal that laser hardening by using diode laser will cause larger geometrical dimensions and higher microhardness than CO<sub>2</sub> laser. Pinahin et al. [10] presented the appropriate process for increasing wear resistance and mechanical behavior of several hard alloys including VK6, VK8, T5K10, and T15K6 using pulsed laser hardening. In this study the wear resistance increases 1.2 times by laser hardening process. Effects of laser hardening process parameters including laser power and scanning speed were investigated on 4Kh5MFS steel without surface melting by Aborkin et al. [11]. Microhardness value, maximum hardness and surface quality were evaluated. The range of the depth of hardness, the maximum hardness and the surface roughness in this study were 0.66-0.86 mm, 675-750 Hv and 0.6-1.2 μm, respectively. CO<sub>2</sub> laser with long pulses was used for laser surface melting hardening of C80U steel by Bien et al. [12]. The plasma generated by laser in the process was validated through a high-speed camera. The hardness of the material in laser melting process reach to 1222.8 Hv from 240 Hv of the base material. The wear and corrosion behavior of AISI H13 tools steel were studied by Telesang et al. [13] after conducting the 6 kW high power diode laser surface hardening process. The microhardness increased to 810 Hv while the hardness of the base material was 500 Hv. Corrosion resistance in NaCl 3.56% solution of the laser hardened sample increased in comparison of the base

material, -960mV SCE and -920mV SCE, respectively. The laser energy of 75 J/mm<sup>2</sup> has the higher tribology improvement of the material. Numerical and experimental study of the Nd:YAG laser surface hardening with overlapped tracks of AISI 4140 low alloy steel was investigated [14]. Geometrical dimensions of the hardened zone and microhardness distribution were analyzed. Their finite element method validated by conducting experimental tests and it showed a good agreement. High power diode laser surface hardening of low carbon steel AISI 1040 carried out to improve the fatigue life by Guarino et al. [15]. Effects of each laser process parameter studied on the rotating bending fatigue tests of laser treated components. Wohler curves showed that laser surface hardening significantly increase the fatigue life and mechanical properties of the treated samples. More recently Moradi et al. [16] investigated laser surface hardening of martensitic stainless steel AISI 420 by a 1.6 kW high power diode laser. Effects of process parameters on geometrical dimensions, microhardness distribution, and microstructure were studied. They could increase the surface hardness to 720 Hv from 210 Hv and the dimension of hardened layer was 1.2 mm in depth and 6.1 mm in width.

In spite of the efforts of these, and other researchers, many aspects of laser hardening of steel alloys are still unsolved and more research needs to be carried out with the aim of increasing the hardness values reached and the depth of the hardened layer. The application of Diode lasers to hardening is a relatively new addition to this field. In this study, the DOE technique known as Response Surface Methodology (RSM) is used in conjunction with Design Expert software to analyze the effect of diode laser surface hardening process parameters (incident beam size, scanning speed and laser power) on the geometry and hardness of hardened layers created on AISI 4130 carbon steel. From the results Optimum parameters were established and validated by experiment. Finally, the effect of partially overlapping hardened tracks was investigated from a production engineering and metallurgical point of view.

## **2. Experimental design and methodology**

### ***2.1. Response surface methodology (RSM)***

Design of experiments (DOE) involves a series of experiments that deliberately modify the input variables of the process to be observed and then detect the variation in the output response of the process [17-19]. Response Surface Methodology (RSM) is a mathematical and statistical methods which are valuable for analyzing and modeling issues affected by several variables and aims to optimize the response [20, 21]. In most issues related to RSM,

the relationship between the output response and the independent variables is unknown. For this reason the first step in Response Surface Methodology is to find approximations for the actual relationship between the responses and the set of independent variables. Usually, low-order polynomials are used with independent variables. If there is any curvature in the system then higher-order polynomials need to be used. Equation 1 presents the general form of the polynomial equation [22];

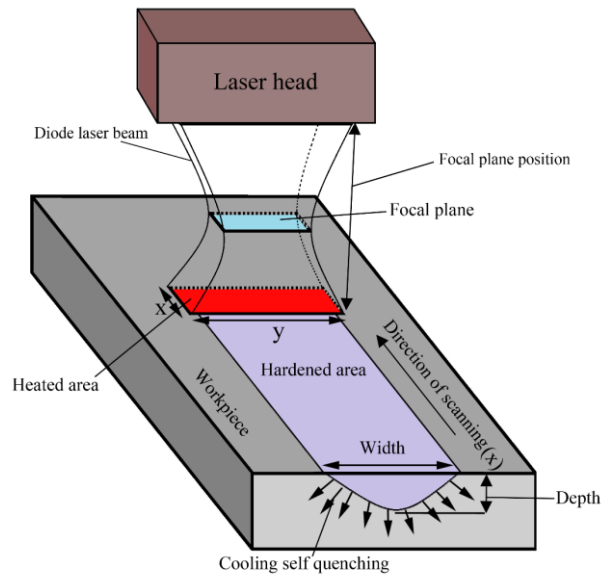
$$y = \beta_0 + \sum_{i=1}^k \beta_i x_i + \sum_{i=1}^k \beta_{ii} x_i^2 + \sum_i \sum_j \beta_{ij} x_i x_j + \varepsilon \quad (1)$$

In the above equation,  $\beta$  is a constant,  $\beta_i$  is a linear coefficient,  $\beta_{ii}$  is a quadratic coefficient,  $\beta_{ij}$  is an interaction coefficient and  $\varepsilon$  is the error of the parameters of the regression. In almost all responses, one or some of these approximation polynomials are used. Of course, it is unlikely that a polynomial model will be a reasonable approximation of the real relationship in the total variable space, but for a relatively small region such models usually work well [23].

In this research the scanning speed (S), focal plane position (FPP), and the laser power (P) were considered as independent input variables. Three input parameters of the experiment, giving coded values and actual values depicted in [Table 1](#). [Figure 1](#) presents a schematic which clarifies the effect of changing the distance between the focal position and the surface of the workpiece. The beam incident on the sample surface is rectangular in cross section and increasing the focus-material distance increases the beam size in both the direction of travel (x) and perpendicular to that direction (y). The FPP = 60 mm means that the focal plane is exactly positioned on the material surface. The dimensions of the beam for each focal plane position used here are given in [Table 2](#). Central composite design (CCD) of five-level RSM with three parameters was applied in the present work. This experimental design includes 17 experiments; six as axial points, eight as factorial points in the cubic vertex, and three in the cubic centre. [Figure 2](#) illustrates the cubic space with design levels (-2 to +2) for the three varied parameters, according to the design matrix (see [Table 1](#)).

**Table 1.** Independent process parameters with design levels.

Variable	Symbol	Unit	-2	-1	0	1	2
Scanning Speed	S	[mm/s]	3	4	5	6	7
Laser Power	P	[w]	1200	1300	1400	1500	1600
Focal Plane Position	FPP	[mm]	60	65	70	75	80

**Figure 1** a schematic of the laser surface hardening process**Table 2.** The relationship between the Incident Beam Length, Width and Area.

Focal Plane Position	Incident Beam Length (x)	Incident Beam Width (y)	Incident Beam Area (xy)
60 mm	1.50 mm	8.00 mm	12.00 mm <sup>2</sup>
65 mm	2.55 mm	9.94 mm	25.34 mm <sup>2</sup>
70 mm	3.60 mm	11.88 mm	42.77 mm <sup>2</sup>
75 mm	4.65 mm	13.82 mm	64.30 mm <sup>2</sup>
80 mm	5.67 mm	15.76 mm	89.36 mm <sup>2</sup>

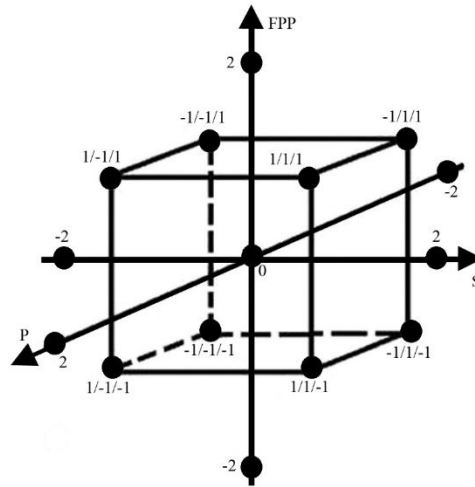


**Figure 2.** Cubic space with the design levels (-2 to +2)

## 2.2 Experimental Work

AISI 4130 carbon steel was the subject of this study. The chemical composition of the material presented in [Table 3](#), is the average of three X-ray fluorescence (XRF) measurements. 10mm thick samples were cut from 65 mm diameter rod and surface ground before heat treatment.

**Table 3.** Chemical composition of AISI 4130 carbon steel (Wt. %)

C	Si	Ni	Mn	P	S	Cu	Cr	Mo	Al	V	Fe
0.25	0.3	0.05	0.87	0.016	0.03	0.06	1.01	0.25	0.024	0.012	Balance

A diode continuous wave laser with a maximum power of 1600 W was used as the laser source. The wavelength of the used diode laser is 808 nm. Initial trial specimens were produced to define the working range of each input parameter. Laser hardening experiments were then carried out according to the matrix design presented in [Table 4](#) in which an overview of the results of the experiments is illustrated. The interaction time is calculated by dividing the incident beam length ( $x$ ) to the scanning speed ( $S$ ), Equation 2. Incident Beam Length ( $x$ ) is presented in [Figure 1](#) and [Table 2](#). By dividing the laser power to the incident beam area, presented in [Table 2](#), the beam density will be obtained, Equation 3 [24].

$$\text{Interaction time} = \text{Incident beam length (x)} / \text{Scanning speed (S)} \quad (2)$$

$$\text{Beam density} = \text{Laser power} / \text{Incident beam area} \quad (3)$$

**Table 4.** Results overview

Sample No.	Input variables (Coded values)			Output responses							
	Scanning Speed (mm/s)	Laser Power (W)	Focal Plane Position (mm)	Max Depth of hardened layer (mm)	Width of hardened layer (mm)	Angle (°)	Average Surface Hardness	Average Hardness	Ferrite percent (%)	Beam Density W/mm <sup>2</sup>	Interaction Time (s)
1	4	1500	65	0.94	9.3	10.82	586	553	0.22	59.2	0.64
2	7	1400	70	0.22	8.86	3.04	342	388	14.21	32.7	0.5
3	5	1400	70	0.47	9.82	5.95	498	514	0.47	32.7	0.7
4	5	1400	70	0.44	9.84	5.89	480	458	0.49	32.7	0.7
5	5	1400	60	1.02	9.78	13.02	577	643	0.18	117.	0.3
6	5	1400	80	0.30	9.97	4.29	370	391	9.4	15.7	1.13
7	6	1300	75	0.27	8.73	4.06	338	392	9.62	20.2	0.8
8	6	1300	65	0.42	9.03	7.02	424	536	0.6	51.3	0.4
9	4	1300	75	0.39	9.24	5.24	386	442	0.62	20.2	1.16
10	4	1300	65	0.52	9.10	6.78	549	525	0.27	51.3	0.6
11	6	1500	65	0.50	9.27	6.57	544	517	0.41	59.2	0.4
12	5	1400	70	0.43	9.85	5.7	400	450	0.55	32.7	0.7
13	5	1600	70	0.52	10.1	6.47	542	611	0.26	37.4	0.7
14	6	1500	75	0.34	9.24	4.47	356	402	1.29	23.3	0.8
15	3	1400	70	0.48	9.37	6.02	496	544	0.45	32.7	1.2
16	5	1200	70	0.23	8.58	3.72	330	345	10.73	28.1	0.7
17	4	1500	75	0.62	9.86	8.21	474	508	0.25	23.3	1.16

**Fig. 3** shows typical cross section results of hardened track produced with various parameter settings. After laser hardening each sample was sectioned perpendicular to the hardened line. In order to prepare the metallographic samples, cut specimens were mounted in phenolic resin, polished and etched in 2% Nital [25]. The geometric features of the hardened layer (width and depth), **Fig. 4**, were measured using a BUEHLER MET B7 optical microscope and the images were analyzed by ImageJ software. The microstructure was analysed by optical microscopy (OM) and field emission scanning electron microscopy (FE-SEM).

Celemex software was used to measure the percentage of ferrite in the structure of the hardened layer. Microhardness measurements (Micro Hardness V-Test-analog) were accomplished along a line 50  $\mu\text{m}$  below the top surface on the transversal cross section of the hardened zone. These measurements were taken by a maximum load of 100g and a dwell time of 30 seconds, the microhardness tests were repeated at least three times for each sample and in each case ten measurements were taken. Hardness profiles were also produced along the vertical center line from the top surface to the base metal below the hardened zone. The hardness of the untreated steel was 265Hv.

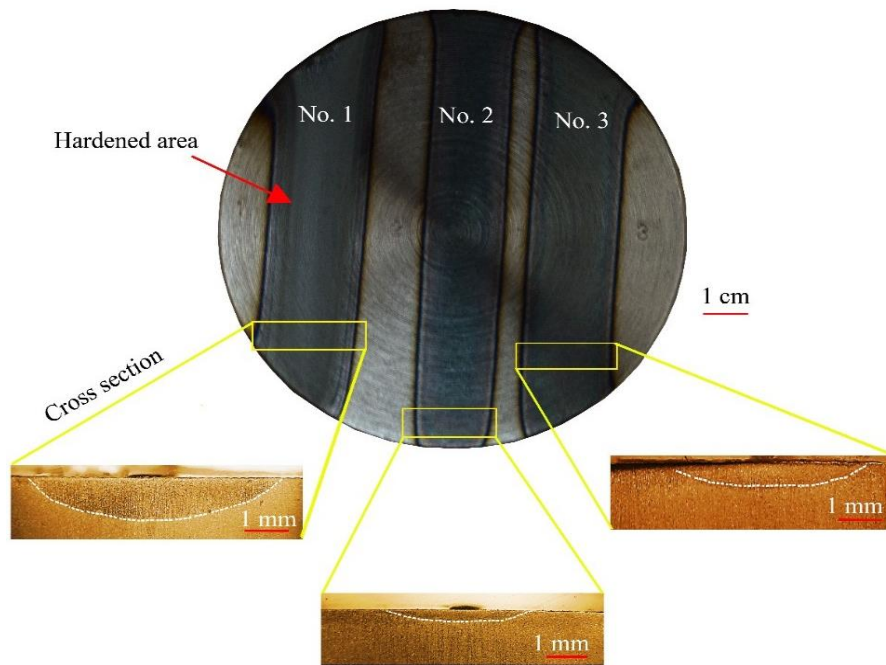


**Figure 3** Image of laser hardened samples (sample diameter is 65mm)

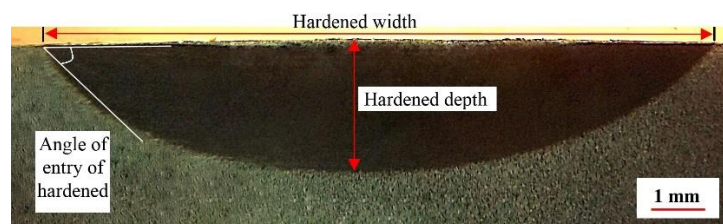


**Figure 4.** Schematic of geometrical dimensions of hardened zone (width, depth and angle)

### 3. Results and discussion

The geometrical dimensions of the hardened zone (width, depth, and angle) and its hardness (general average and average surface hardness) were measured as the output responses of the experiment. Analysis of variance (ANOVA) was applied to investigate significant parameters and their effects. In these analyses, full quadratic polynomial functions were employed using Design Expert software. The results presented in [table 4](#) can now be analyzed to give information about the width, depth and hardness of the hardened tracks created, as a function of the changes in process parameters.

### 3.1 Depth of hardened layer

Table 5 shows analysis of variance for the depth of hardened layer. As shown in Table 5, all the main parameters are effective. Among quadratic terms, only the quadratic term of focal plane position (FPP<sup>2</sup>) and interaction effect of focal plane position and scanning speed (S×FPP) were identified as the significant term. According to performed analyses in ANOVA Table 5, equation 4 & 5 represents the regression equation for the depth of hardened layer considering significant parameters based on coded and actual values, respectively.

$$(\text{Max Depth of hardened track})^{0.05} = 0.96 - 0.020 S + 0.019 P - 0.024 \text{ FPP} + 0.019 \text{ FPP}^2 \quad (4)$$

$$(\text{Max Depth of hardened track})^{0.05} = 0.97294 - 0.010080 S + 9.25339\text{E-}005 P - 0.042344 \text{ FPP} + 4.28922\text{E-}003 \text{ FPP}^2 \quad (5)$$

**Table 5** Revised ANOVA of the depth of hardened layer

Source	Sum of Squares	Degree of freedom	Mean Square	F-value	P-value
Model	6.43	5	1.29	23.22	< 0.0001
S	1.61	1	1.61	29.12	0.0002
P	1.42	1	1.42	25.56	0.0004
FPP	2.53	1	2.53	45.67	< 0.0001
S×P	0.19	1	0.19	3.43	0.0911
FPP <sup>2</sup>	0.68	1	0.68	12.35	0.0048
Residual	0.61	11	0.055		
Lack of Fit	0.60	9	0.067	17.66	0.0547
Pure Error	7.571E-003	2	3.785E-003		
Total	70.04	16			
R-Squared= %91.35			R-Squared (Adj)= %87.41		

Fig. 5 depicts perturbation plot of depth of hardened layer. The perturbation plot can help to compare the effect of all the factors in the central point in the design space. The depth of hardened layer is plotted by varying only one parameter over its range while the other factors are kept fix. Each line in the plot shows the sensitivity of depth of hardened layer to the input variables. From the perturbation plot it is crystal clear that the laser power has direct effect while the focal plane position and the scanning speed have reverse effect on the depth of hardened layer. This relation could be easily understood from the physical phenomena of laser hardening process.

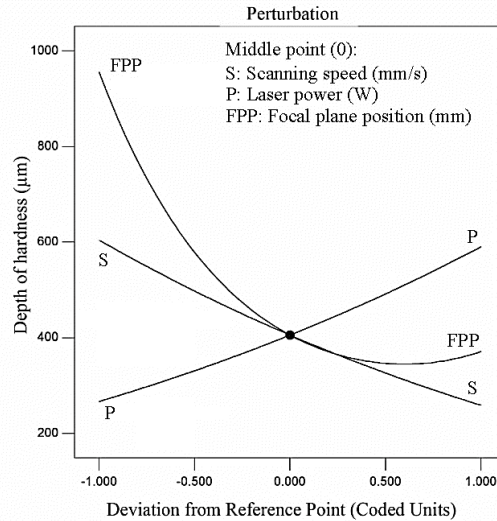


**Figure 5** Perturbation plot of depth of hardened layer

Fig.6 illustrates the depth of hardened layer response surface based on the input parameters. Fig 6-a shows the relation of the laser power and the scanning speed on the depth of hardness. The heat input presented in Equation (6) is used for better understanding of the process and explaining this phenomenon.

$$\text{Heat input} = \text{Laser power} / \text{Scanning Speed} \quad (6)$$

Thus heat input increases when the laser power increases and the scanning speed decreases. By reducing the scanning speed the interaction time of the laser and material will be enhanced. Then more part of the surface of the material will be heated and the depth of hardened layer increases.

Fig 6-b depicts the behavior of the depth of hardness in relation with the focal plane position and the scanning speed. By considering the concept of the beam density presented in Table 4 which is a function of the incident beam area presented in Table 2 the red area in Figure 1, Figure 6-b could be more understandable. While the focal plane position reduces the incident beam area will be smaller and the beam density will be increases. Also the effect of the scanning speed is mentioned in the above paragraph. Based on these explanations we could see that reducing the position of the laser focal plane and the scanning speed will increase the depth of hardened layer.

According to Fig. 6-c while the laser power increases and the focal plane position reduces the depth of hardened layer increases. It is because of the beam density relation. Reduction the FPP causes smaller incident beam area and while the power increases the energy beam density will be increases. Thus the more energy transferred to the material and the depth of hardened layer increases.

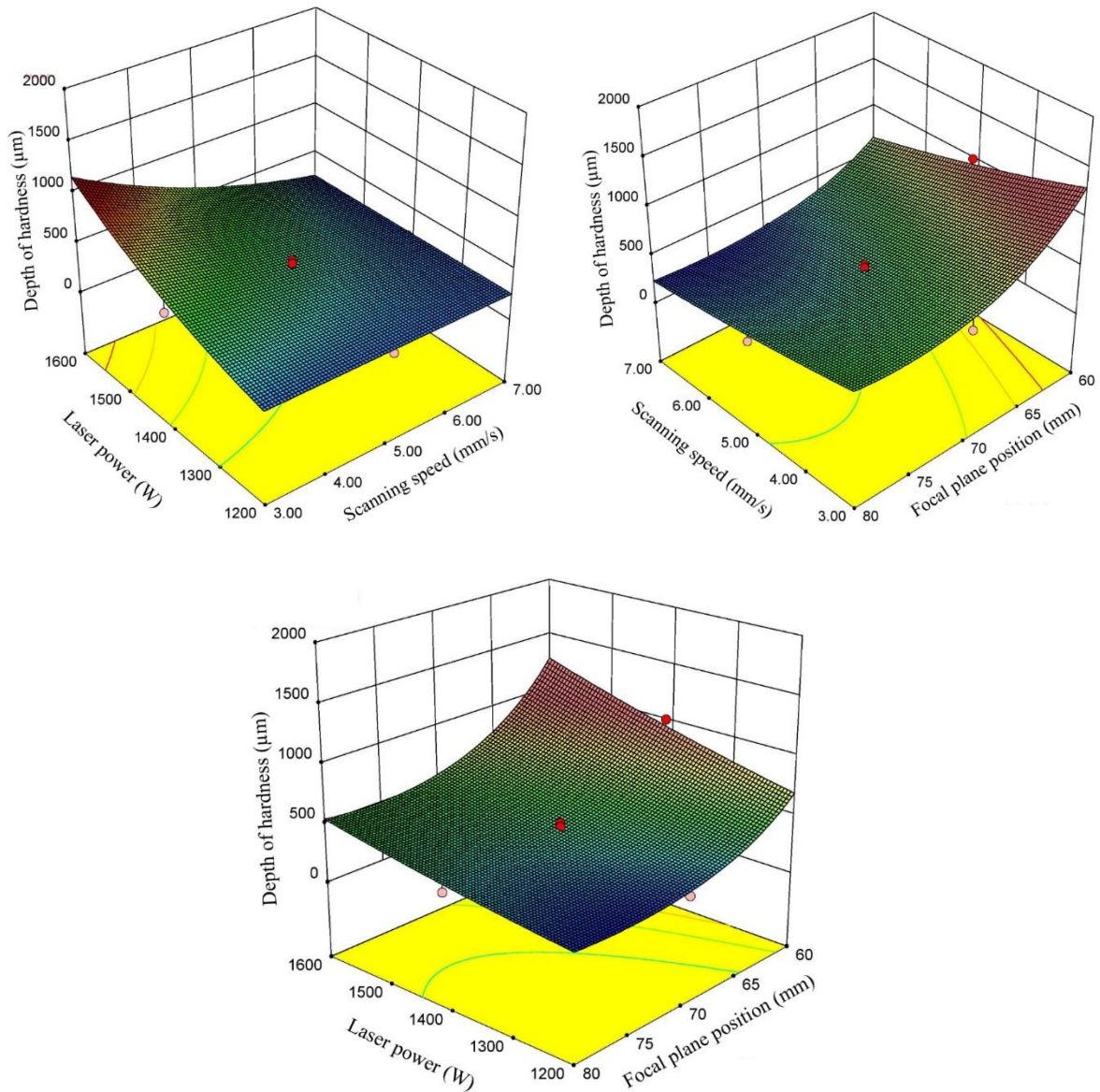


**Figure. 6** Response surfaces of depth of hardened layer in terms of input variables

### 3.2 Hardened track width

The width of the hardened track created by any set of process parameters is of great importance because the width multiplied by the process velocity is equal to the coverage rate of the process. According to analysis of variance on hardened track width, [Table \(6\)](#), the effective parameters which are linear, are laser power (P), scanning speed (S). Among quadratic terms, the quadratic term of the laser power ( $P^2$ ) and the scanning speed ( $S^2$ ) have a significant effect.

**Table 6** Revised ANOVA of the hardened track width

Source	Sum of Squares	Degree of freedom	Mean Square	F-value	P-value
Model	4.372E-007	4	1.093E-007	12.39	0.0003
S	5.610E-008	1	5.610E-008	6.36	0.0268
P	2.189E-007	1	2.189E-007	24.82	0.0003
S <sup>2</sup>	1.224E-007	1	1.224E-007	13.88	0.0029
P <sup>2</sup>	8.425E-008	1	8.425E-008	9.55	0.0094
Residual	1.059E-007	12	8.822E-009		
Lack of Fit	1.058E-007	10	1.058E-008	440.82	0.0023
Pure Error	4.801E-011	2	2.400E-011		
Total	5.431E-007	16			
R-Squared= 80.51 %			R-Squared (Adj)= 74.01 %		

Pursuant to the statistical analysis, the regression equation in terms of coded and actual variables values are presented in equation (7) and (8), respectively.

$$(\text{Width of hardened track})^{-3} = 1.092\text{E-}003 + 1.184\text{E-}004 S - 2.339\text{E-}004 P + 2.922\text{E-}004 S^2 + 2.424\text{E-}004 P^2 \quad (7)$$

$$(\text{Width of hardened track})^{-3} = 0.016137 - 6.71232\text{E-}004 S - 1.81371\text{E-}005 P + 7.30448\text{E-}005 S^2 + 6.05978\text{E-}009 P^2 \quad (8)$$

Figure 7 depicts the response surface graphs for the track width as a function of the scanning speed and the laser power. This graph is interpolated by the data and it is based on regression equation 7 and 8.

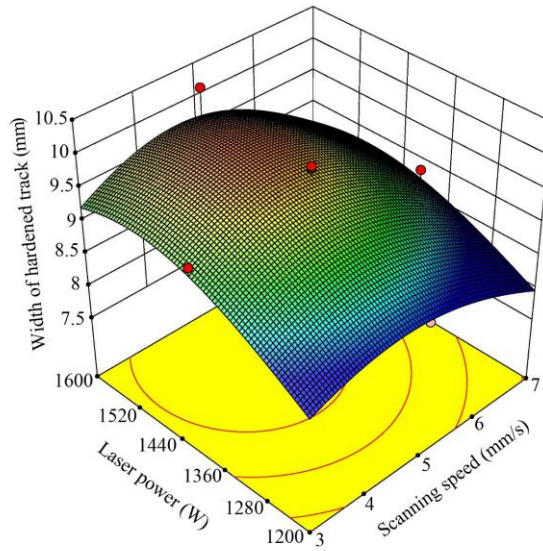


**Figure. 7** The response surface graph of width of hardened layer in terms of the scanning speed and the laser power

The response surface graph presented in Fig 7 show that by decreasing the scanning speed and increasing the laser power, the heat input increases (see Equation 6) and the area of the material which is heated by the laser beam will be increases, therefore the width of hardened layer will become wider.

### 3.3 Angle of entry hardened profile

Table 7 demonstrates the ANOVA for the angle of entry hardened profile. As presented in Table 7 all of the main linear parameters are effective. Among quadratic terms, the quadratic term of laser power ( $P^2$ ) has a significant effect and the only effective interaction is interaction of the laser focal plane position and the scanning speed ( $S \times FPP$ ). According to conducted analyses in ANOVA table 7 equation 9 and 10 indicates the regression relation for the angle of entry hardened profile considering effective terms based on coded and actual values, respectively:

$$(\text{Angle})^{0.5} = +2.33 - 0.39 S + 0.31 P - 0.61 FPP - 0.62 S \times P + 0.58 FPP^2 \quad (9)$$

$$(\text{Angle})^{0.5} = +22.65576 + 1.98999 S + 9.37013E-003 P - 0.86629 FPP - 1.56097E-003 S \times P + 5.75058E-003 FPP^2 \quad (10)$$

**Table 7** Revised ANOVA of the angle of entry hardened profile

Source	Sum of Squares	Degree of freedom	Mean square	F-value	P-value
Model	3.21	5	0.64	21.28	< 0.0001
S	0.61	1	0.61	20.23	0.0009
P	0.39	1	0.39	12.99	0.0041
FPP	1.50	1	1.50	49.64	< 0.0001
S×P	0.19	1	0.19	6.46	0.0274
FPP <sup>2</sup>	0.52	1	0.52	17.08	0.0017
Residual	0.33	11	0.030		
Lack of Fit	0.33	9	0.037	50.18	0.0197
Pure Error	1.464E-003	2	7.320E-004		
Total	3.54	16			

---

R-Squared= %90.63	R-Squared (Adj)= %86.37
-------------------	-------------------------

Fig. 8 depicts perturbation plot of angle of entry hardened profile. This perturbation graph is similar to the Fig. 8, the perturbation plot of the depth of hardening. As mentioned for explanation of the Fig. 8 the scanning speed and the focal plane position have reverse effect while the laser power has direct effect on the angle of entry.

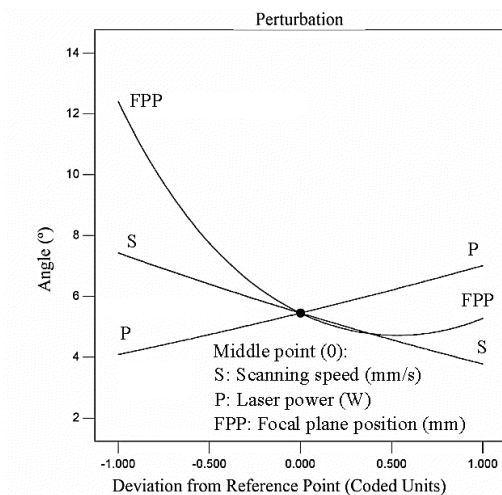


**Figure. 8** Perturbation plot of angle of entry hardened profile

Fig. 9 illustrates the angle of entry hardened profile response surface in terms of input variables. In all the 3D plots of Fig 9 we see the same trend of the parameters like Fig. 6. Beam density, interaction time, and heat input of the process which affect the geometrical

dimensions of the hardened zone, are used for explaining how process parameters influence the angle of entry. The same descriptions mentioned in section 3.1 could be used for explaining the trend of the parameters effects on the angle of entry. The larger angle means that the hardened area will be closer to the rectangular shape which is more desired for laser hardening process while most of other laser hardening process by other lasers are triangle shape. It is one of the other advantages of the surface hardening by diode laser.

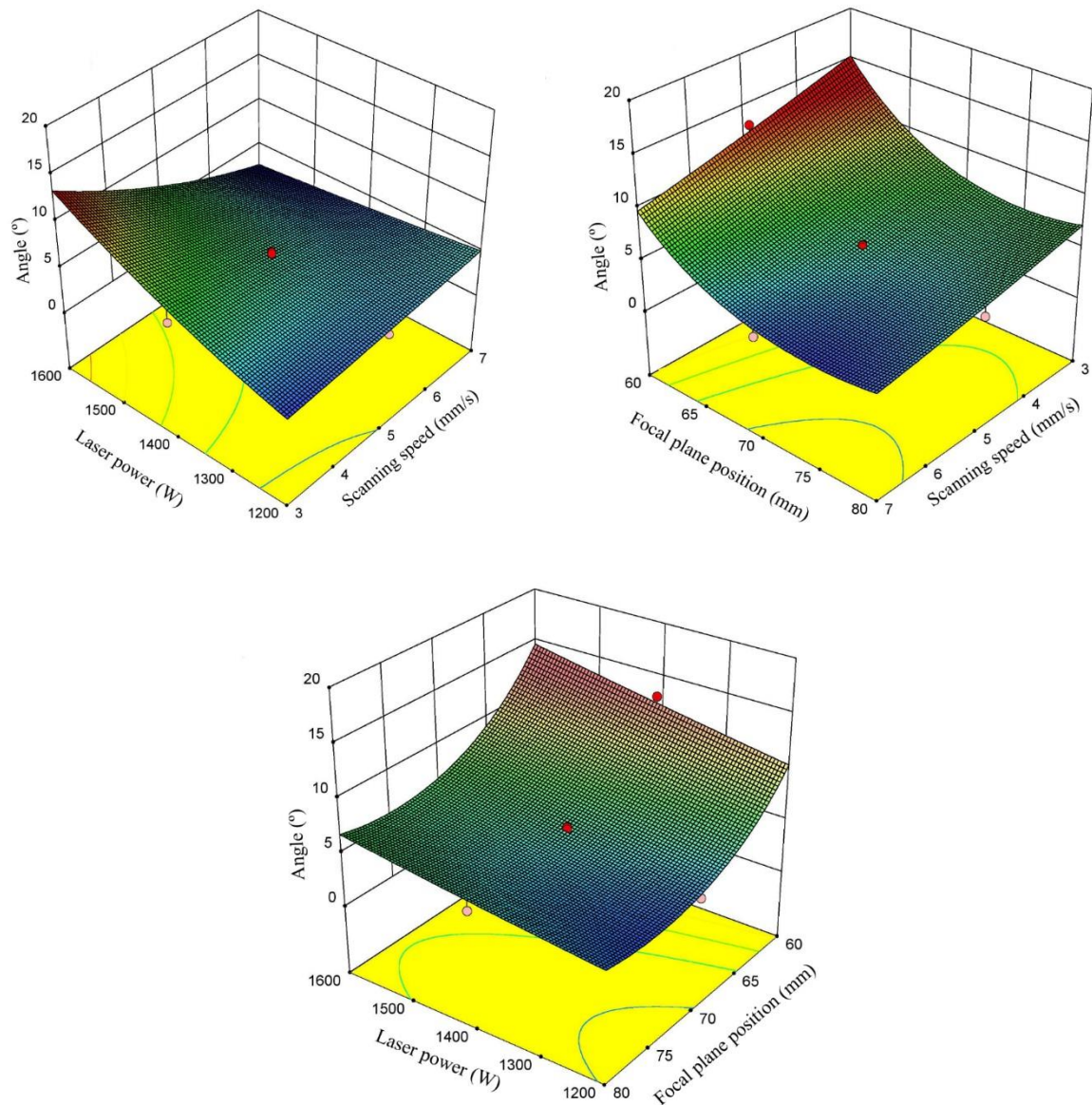


**Figure. 9** Response surface plot of angle of entry hardened profile in terms of input parameters

### 3.4 Average surface hardness

After measuring the microhardness in different points under the hardened layer the average surface hardness calculated as mentioned in experimental work section. ANOVA [Table 8](#) demonstrates the results of data statistical analysis of the average surface hardness. All the

main parameters are significant but none of the quadratic and interaction effects are significant.

**Table 8.** Revised ANOVA of the average surface hardness

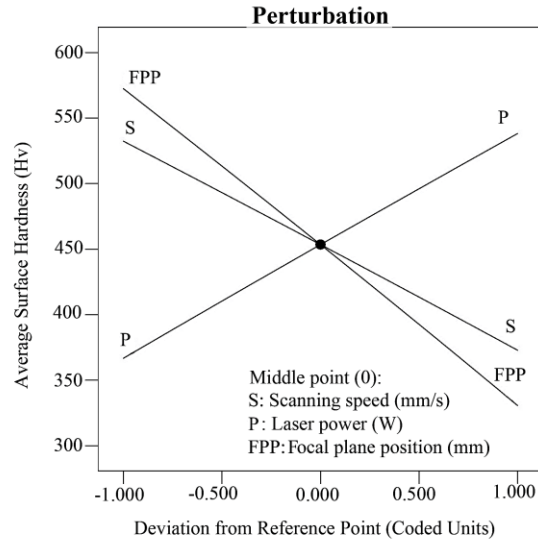
Source	Sum of Squares	Degree of freedom	Mean Square	F-value	P-value
Model	6.152E+005	3	2.051E005	31.78	< 0.0001
S	1.383E+005	1	1.383E+005	21.43	0.0005
P	1.598E+005	1	1.598E+005	24.77	0.0003
FPP	3.171E+005	1	3.171E+005	49.14	< 0.0001
Residual	83889.46	13	6453.04		
Lack of Fit	54378.56	11	4943.51	0.34	0.9079
Pure Error	29510.89	2	14755.45		
Total	6.991E+005	16			
R-Squared= 88.00 %			R-Squared (Adj)= 85.23 %		

The equations 11 and 12 are final equations of the average surface hardness in terms of coded and actual values, respectively:

$$(\text{Average Surface Hardness})^{1,12} = 944.81 - 185.94 S + 199.90 P - 281.56 \text{ FPP} \quad (11)$$

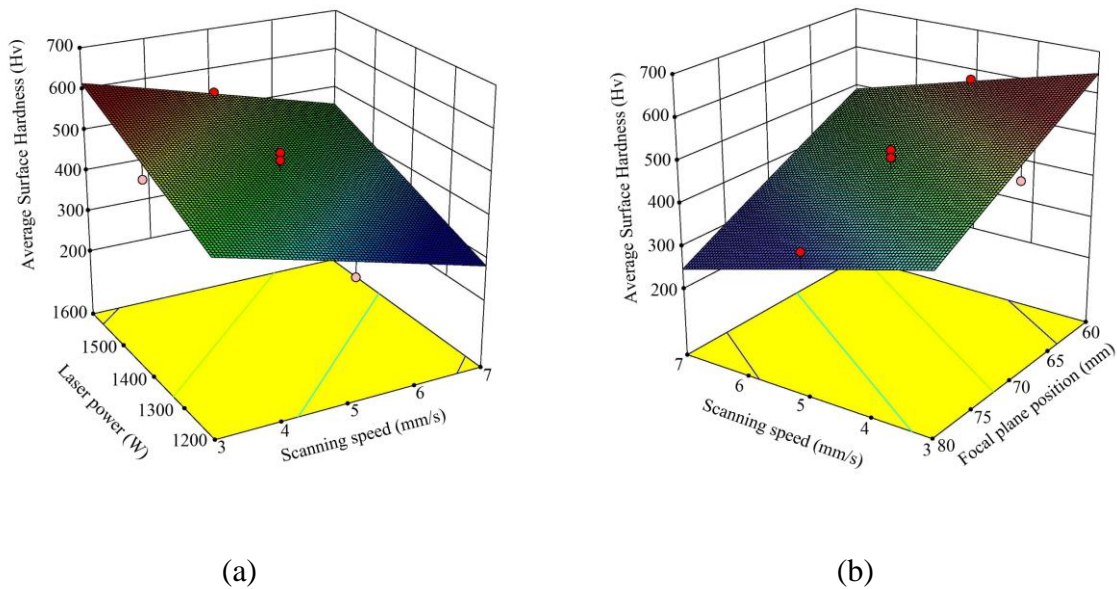
$$(\text{Average Surface Hardness})^{1,12} = 493.03298 - 92.97145 S + 0.99951 P - 134.07555 \text{ FPP} \quad (12)$$

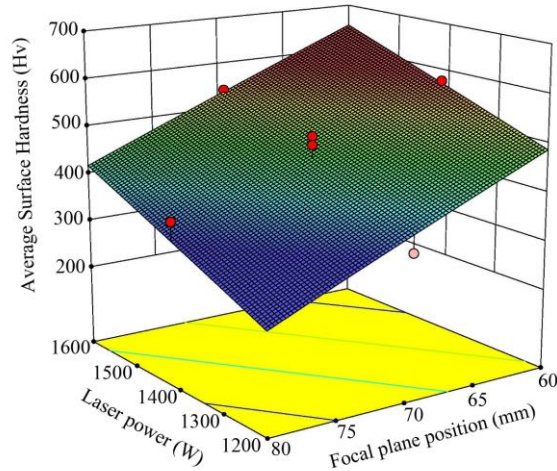
The power of the regression Equations (11,12), is calculated by Box-Cox method which is one of the basic statistical analyzing approach for better modelling. Application of this method will minimize the sum of square error. Perturbation plot of average surface hardness is depicted in Fig 10. The trend of the parameters effect are similar to the previous perturbation plots but linearly in this case because of the linear regression equation.



**Figure. 10.** Perturbation plot of average surface hardness

Fig. 11 demonstrates the 3D response surfaces of the average surface hardness in terms of input parameters. The trend of the parameters effects on the average surface hardness is similar to the previous mention responses (see section 3.1, 3.2, and 3.3). As shown in Fig. (11-a) by decreasing the scanning speed the average surface hardness increased. Decreasing the scanning speed means increasing the interaction time. So the material surface will find more time to interact with the laser beam and the surface will be fully austenite [26, 27]. Quenching with air leads to formation the more martensitic phase. The presence of martensite phase will increase the microhardness. Regarding to the Equation 6 the heat input will be increased while the laser power increases and the scanning speed decreases. In Fig 11-b it is evident that reducing the FPP will lead to increases in beam density and it causes higher average surface hardness. The same explanations could be used for explaining the trend of Fig. 11-c.





(c)

**Figure 11.** Response surface plots of the average surface hardness in terms of input parameters

Fig. 12 displays the micro-hardness distribution profile in width of the laser hardened layer in different setting. Samples # 5 and # 6 have the same laser power and the same scanning speed while their focal plane position parameter is difference. In sample # 5 located in 60 mm above the steel surface while in sample # 6 focal plane position is located 80 mm above the steel surface. In samples # 5 (laser power =1600 W, scanning speed 5 mm/s and focal plane position 70 mm), see Table 4, surface hardness increased up to 792 Vickers. The interaction time and beam density for sample # 5 are 0.3 s and 117 W/mm<sup>2</sup>, respectively while for sample # 6 are 1.13 s and 15.7 W/mm<sup>2</sup> (see Table 4). By multiplying the interaction time to beam density for sample # 5 is 35 and for sample # 6 is 17.75. These numbers show that sample # 5 has higher energy in certain time that sample # 6 which lead to higher hardness distribution.

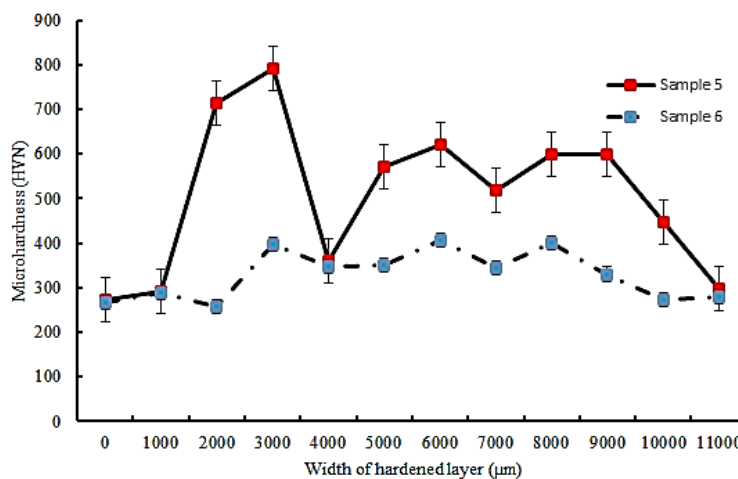


**Figure. 12** Microhardness distribution profile in width of the laser hardened layer

### 3.5 Average hardness in Depth

The average hardness in depth statistical analysis is presented in ANOVA [Table 9](#). As shown in this Table the only effective terms are the main parameters. Based on the statistical analysis, the final regression in terms of coded and actual parameters values presented in Equation. (13 and 14), respectively:

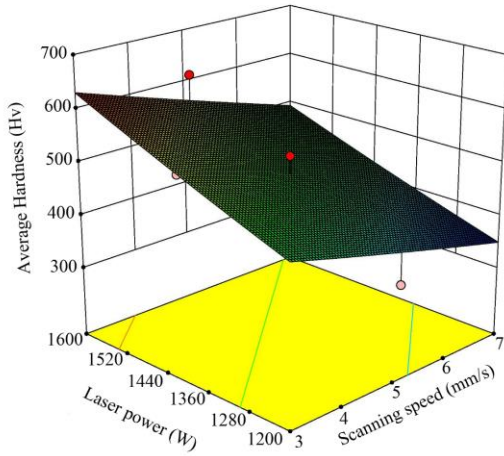
$$(\text{Average Hardness in depth})^{0.51} = 23.31 - 1.56 S + 1.93 P - 2.72 \text{ FPP} \quad (13)$$

$$(\text{Average Hardness in depth})^{0.51} = 18.35557 - 0.77981 S + 9.65571\text{E-}003 P - 1.29668 \text{ FPP} \quad (14)$$

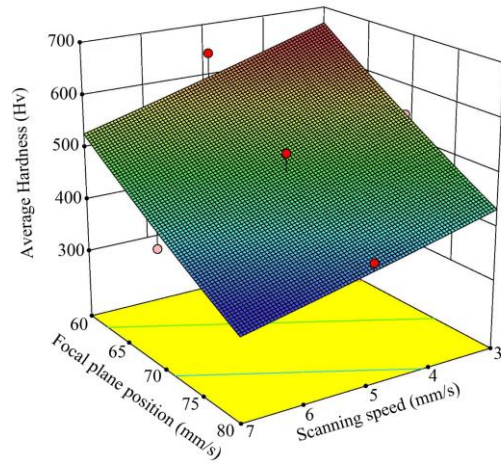
**Table 9.** Revised ANOVA of the Average Hardness in depth

Source	Sum of Squares	Degree of freedom	Mean Square	F-value	P-value
Model	54.31	3	18.10	16.06	0.0001
S	9.73	1	9.73	8.63	0.0115
P	14.92	1	14.92	13.23	0.0030
FPP	29.66	1	29.66	26.31	0.0002
Residual	14.65	13	1.13		
Lack of Fit	13.17	11	1.20	1.62	0.4437
Pure Error	1.48	2	0.74		
Total	68.96	16			
R-Squared= 78.75%			R-Squared (Adj)= 73.85 %		

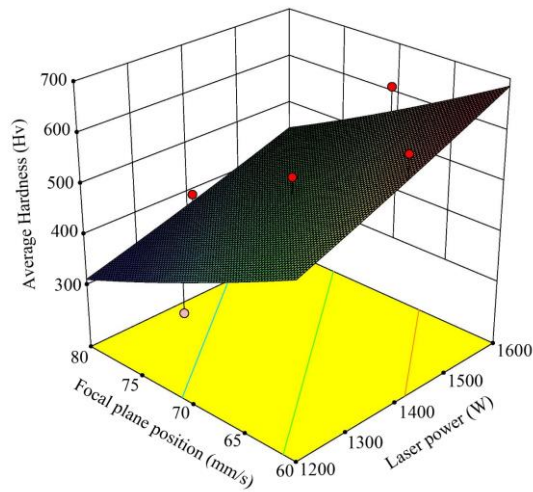
The Average Hardness 3D response surfaces in terms of input parameters are depicted in [Fig. 13](#). The explanation for the average surface hardness in section 3.4 could be used for describing the trend of three plots in [Fig. 10](#). The perturbation plot for the average hardness response is like the one for average surface hardness in section 3.4.



(a)



(b)



(c)

**Figure 13.** Response surface plots of the average hardness in depth in terms of input parameters

Fig. 14 Shows the Microhardness distribution profile in depth of the laser hardened zone in different setting. The reasons explained in section 3.4 for Fig 12 (how the beam density and interaction time effect on the hardness) is the same reason for the trend of the Fig. 14. As seen in Fig. 14 a high difference between the hardness distributions is evident.

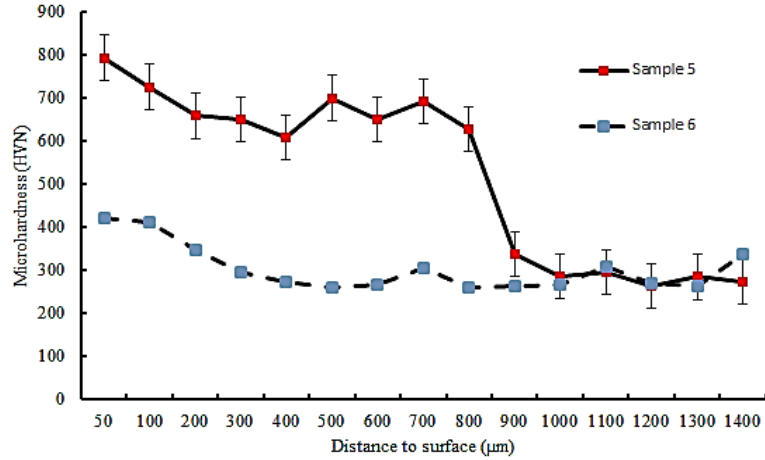


**Fig. 14** Microhardness distribution profile in depth of the laser hardened zone

### 3.6 Ferrite Percentage

Table 10 illustrate the ANOVA for the Ferrite Percentage. As shown in Table 10 only the main linear parameters are effective. Thus according to the statistical analysis, the final regression in terms of coded and actual parameters values yields in Equation. (15 and 16), respectively:

$$(\text{Ferrite percent})^{-0.58} = 1.41 - 0.84 S + 0.75 P - 0.97 \text{ FPP} \quad (15)$$

$$(\text{Ferrite percent})^{-0.58} = -0.068513 - 0.41831 S + 3.73393\text{E-}003 P - 0.46082 \text{ FPP} \quad (16)$$

**Table 10** Revised ANOVA of the ferrite percentage

Source	Sum of Squares	Degree of freedom	Mean Square	F-value	P-value
Model	8.78	3	2.93	25.22	< 0.0001
S	2.80	1	2.80	24.14	0.0003
P	2.23	1	2.23	19.23	0.0007
FPP	3.75	1	3.75	32.29	< 0.0001
Residual	1.51	13	0.12		
Lack of Fit	1.50	11	0.14	27.98	0.0350
Pure Error	9.735E-003	2	4.867E-003		
Total	10.28	16			

---

R-Squared= 85.34%	R-Squared (Adj)= 81.95%
-------------------	-------------------------

---

Fig. 15 depicts perturbation plot of ferrite percentage. From the perturbation plot Fig. 15 it is evident that the laser power has reverse effect while the focal plane position and the scanning speed have direct effect on the ferrite percentage. The effects of all the factors on Ferrite Percentage is exactly reverse comparing their effects on other responses. The scientific reason of this reverse effect is metallurgical concept; having less ferrite percentage in microstructure phases causes more hardness.

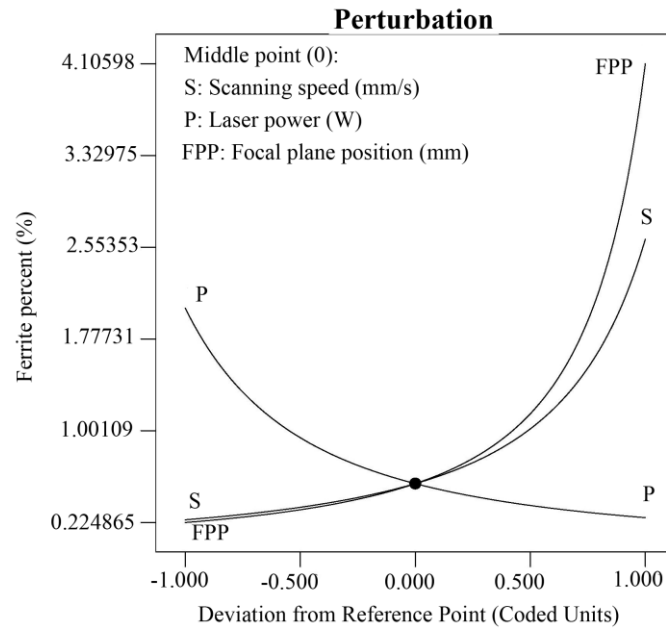


**Figure. 15** Perturbation plot of Ferrite Percentage

#### 4. Optimization

Regression's equations achieved by statistical analyzing the experimental results represent the relations between input parameters and output responses. Desirability function is has been used by the Design Expert statistical software package to optimize the process to reach the desired condition. [23, 26]. Constraints and criteria of the variables and responses are listed in Table 11 to optimize the laser hardening process. The minimum value of Ferrite percent and maximum value of all other responses are the criteria of the optimization in 3 solution presented in Table 11.

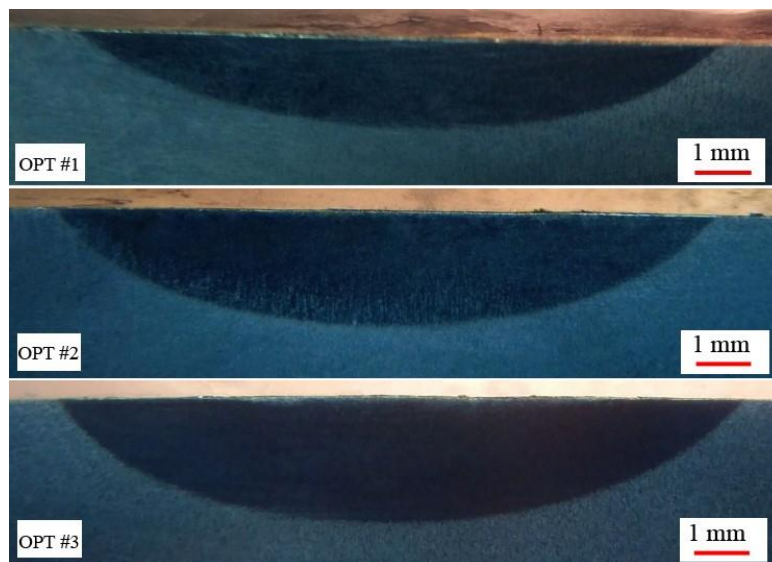
**Table 11** Constraints and criteria of input parameters and responses

Parameter/Response		Goal	Lower	Upper	Importance	
Parameters	Scanning speed	in range	3	7	---	
	Laser power	in range	1200	1600	---	
	Focal plane position	in range	60	80	---	
Response	Criteria 1	Average Surface Hardness	Maximize	330	586	5
		Depth	Maximize	217	1014	5
		Width	Maximize	8583	9972	3
		Ferrite percent	Minimize	0.18	14.21	3
		AEHP	Maximize	3.04	13.02	1
	Criteria 2	Average Surface Hardness	maximize	330	586	5
		Depth	Maximize	217	1014	5
		Width	Maximize	8583	9972	1
		Ferrite percent	Minimize	0.18	14.21	1
	Criteria 3	Average Surface Hardness	Maximize	330	586	5
		Depth	Maximize	217	1009	5
		Ferrite percent	Minimize	0.18	14.21	1

The importance and weight values of the output responses are mentioned in [Table 11](#). For verifying the optimal settings experimental tests are conducted at the optimized results. [Table 12](#) represents the results of the statistical optimization and the experimental ones and the percentage relative verification errors as well. In criteria # 3 of the optimum conditions the surface of the sample is melted. Criteria # 2 is chooses as the best condition of this process because of the better quality and the minimum error. Cross-sectional of laser hardening areas in 3 optimized samples are depicted in [Fig. 16](#).

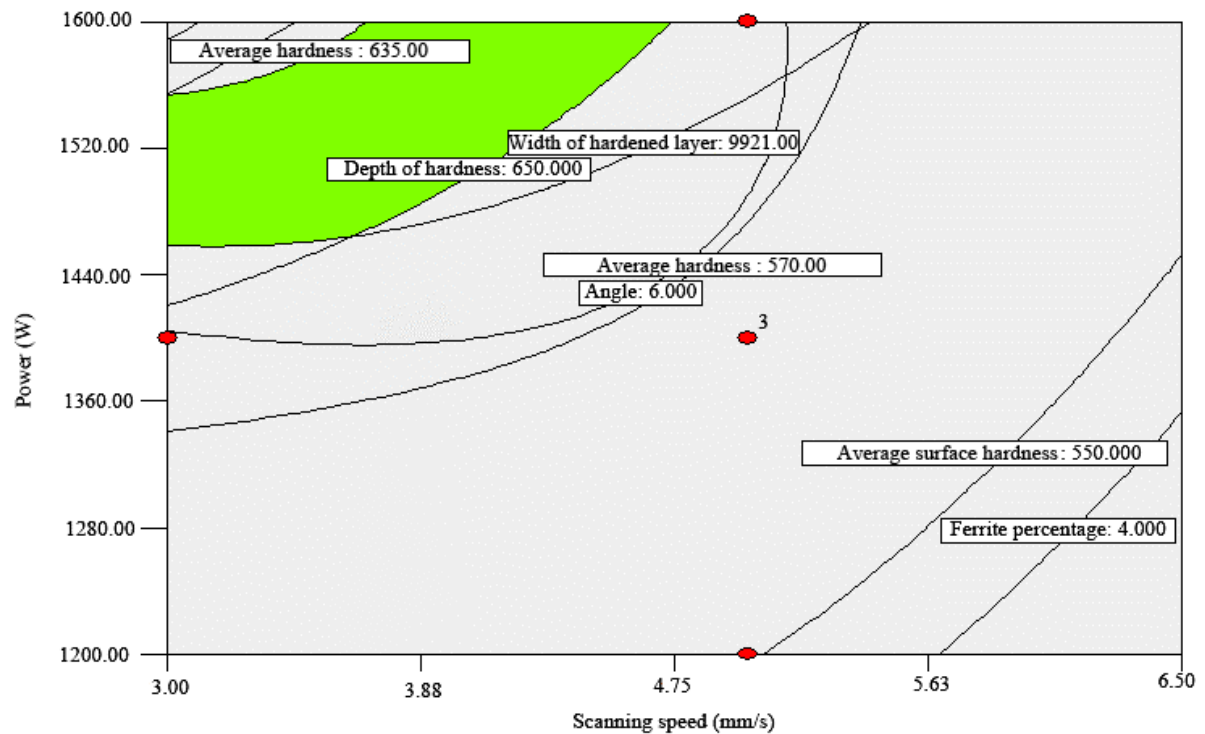
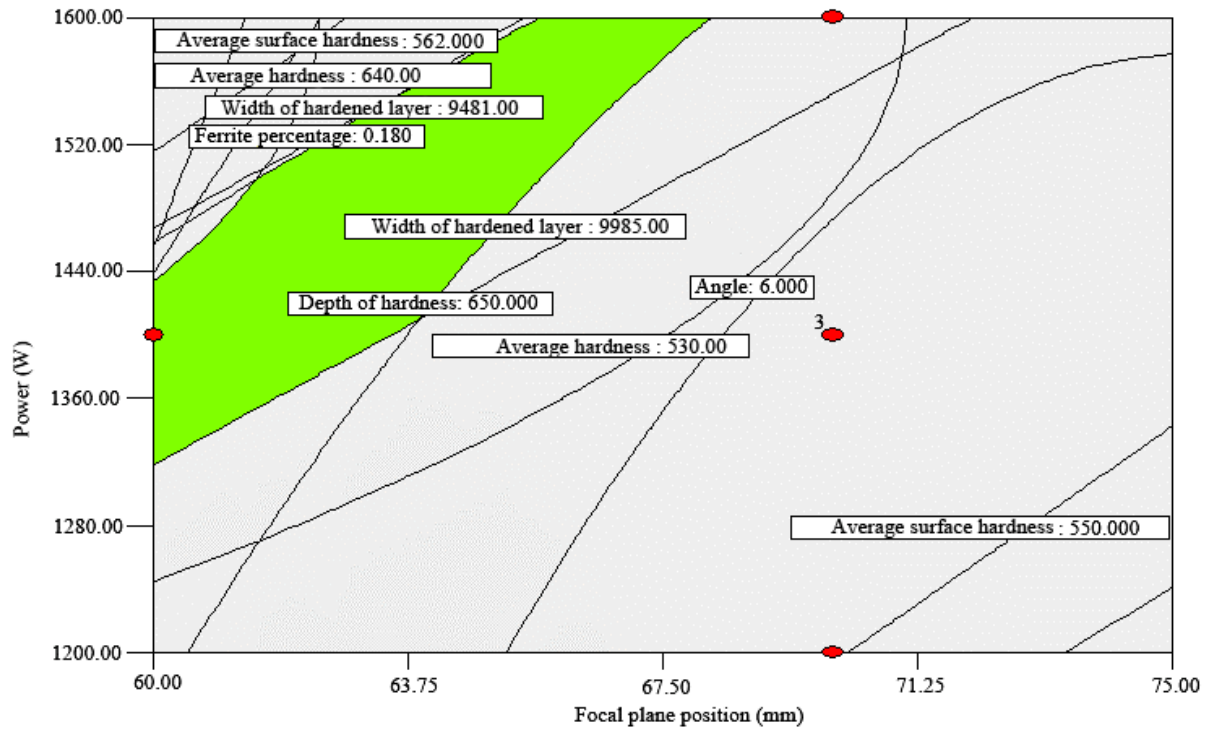
**Table 12** Optimum prediction results and experimental validation

Solution		Optimum input parameters			Composite desirability	Output responses					
		S	FPP	P		Average Surface Hardness	Depth	Width	AEHP	Ferrite percent	
1	Coded value	-1.1	-1.15	1.6	0.8671	Actual	523	957	9451	12.51	0.60
	Actual value	3.9	64.25	1560		Predicted	537	1009.01	9701.66	10.70	0.55
						Error%	2.61%	5.15%	2.65%	14.46%	8.4%
2	Coded value	-0.55	-2	0.91	0.9968	Actual	565	1310	9883	---	0.41
	Actual value	4.45	62	1491		Predicted	578	1129.45	9910.61	---	0.36
						Error%	2.24%	15.98%	0.27%	---	12.19%
3	Coded value	-0.99	-2	2	1	Actual	574	1425	---	---	0.15
	Actual value	4.01	65	1600		Predicted	592	1359.94	---	---	0.13
						Error%	3.04%	4.78%	---	---	13.33%



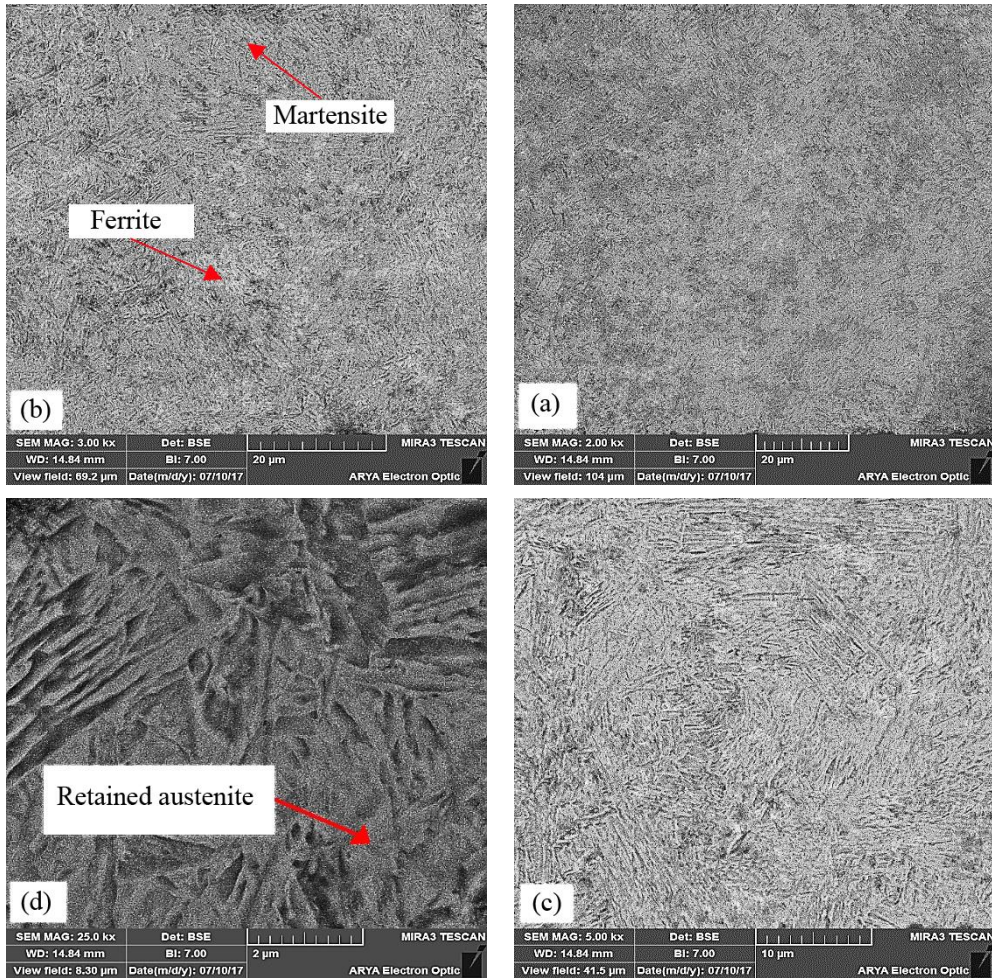
**Figure. 16.** Cross-sectional of laser hardening areas in 3 optimized samples

Fig. 17 depicts overlay plot which contains the contour plots from each output response laid on each other. On each contour plot, the undesirable area is grayed-out. The green area shows that remains defines the final optimal factor settings. As a matter of fact, overly plot suggests an adequate process window to attain the desired condition.



**Figure. 17** Overlay contour plot

Fig. 18 illustrate the microstructure of sample #3 of optimized laser hardening by FESEM in different magnifications in laser hardened layer. Presence of martensite phase in the microstructure lead to increase the hardness value while ferrite phase increase the hardness.



**Figure. 18** Microstructure of sample #3 of optimized laser hardening by FESEM a) magnification 2kx  
 b) Magnification 3kx c) magnification 5kx d) magnification 25kx

## 5. Overlap Test

In the best result # 2 of the optimization (Scanning speed 4.45 mm/s, Focal plane position 62 mm and laser power of 1490 watts) the overlap test were performed. Tow overlap percentages was conducted, 30% and 50%. An immage of the overlap laser hardened samples is illustrated in [Fig. 19](#).

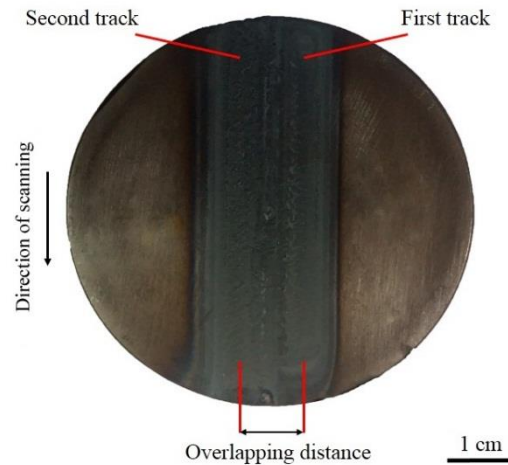


**Figure. 19.** Image of the overlap laser hardened samples (overlap 50%)

Cross section, microhardness distribution, and microstructure of the overlapped laser hardened samples in 50% and 30% are presented in [Figure 20 and 21](#), respectively. [Table 13](#) shows the comparison of characterization of different overlap percentage.

**Table 13.** Comparison of characterization of different overlap percentage

Percentage of Overlap	Width of overlapped ( $\mu\text{m}$ )	Maximum hardness in overlap (HV0.1)	Maximum hardness in the overlap area before overlapping (HV0.1)	Percentage of Ferrite phase (%)	Percentage of Ferrite phase before overlapping (%)
50%	1170	762	483	0.27	9.92
30%	625	681	405	0.38	13.47

As shown in [Table 13](#) in the 50% overlapping it could be explained that in the overlapped area the maximum microhardness increases to 762 Hv while before overlapping the hardness of this area in the first track was 483 Hv. These values for 30% overlapping percentage are 681 HV and 405 Hv, respectively. The increasing of the hardness could be explained by metallurgical concepts. In the first track the surface dose note have enough time for Transformation to austenite phase. Therefore ferrite phase retain in the transformed martensite. In the second track the surface is well-austenite and the ferrite transform to austenite and after the laser quenching martensitic phases appears with the lowest ferrite percentage. The percentage of the ferrite phase in higher overlap percentage is lower which cause the higher hardness. As shown in [Figures 20 and 21](#) and [Table 13](#), the width of overlap area are 1170 micrometers for 50% overlapping and 425 micrometers for 30% overlapping.

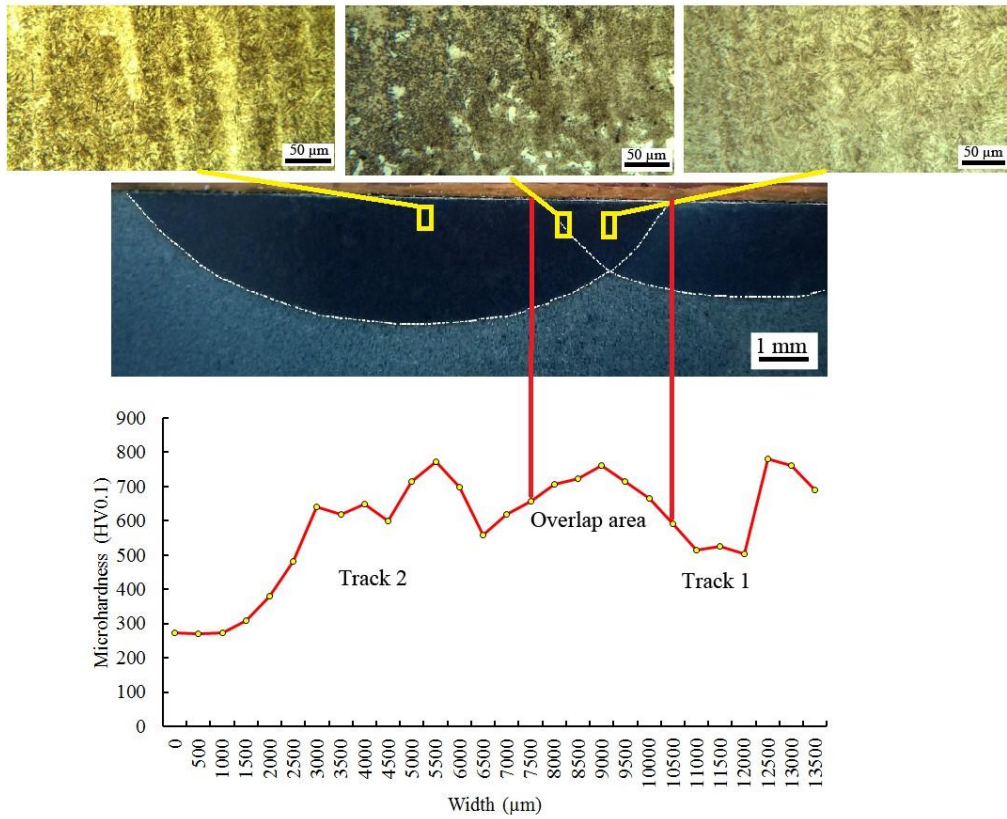


Figure 20. 50% Overlap diagram schematic, microstructure and microhardness distribution

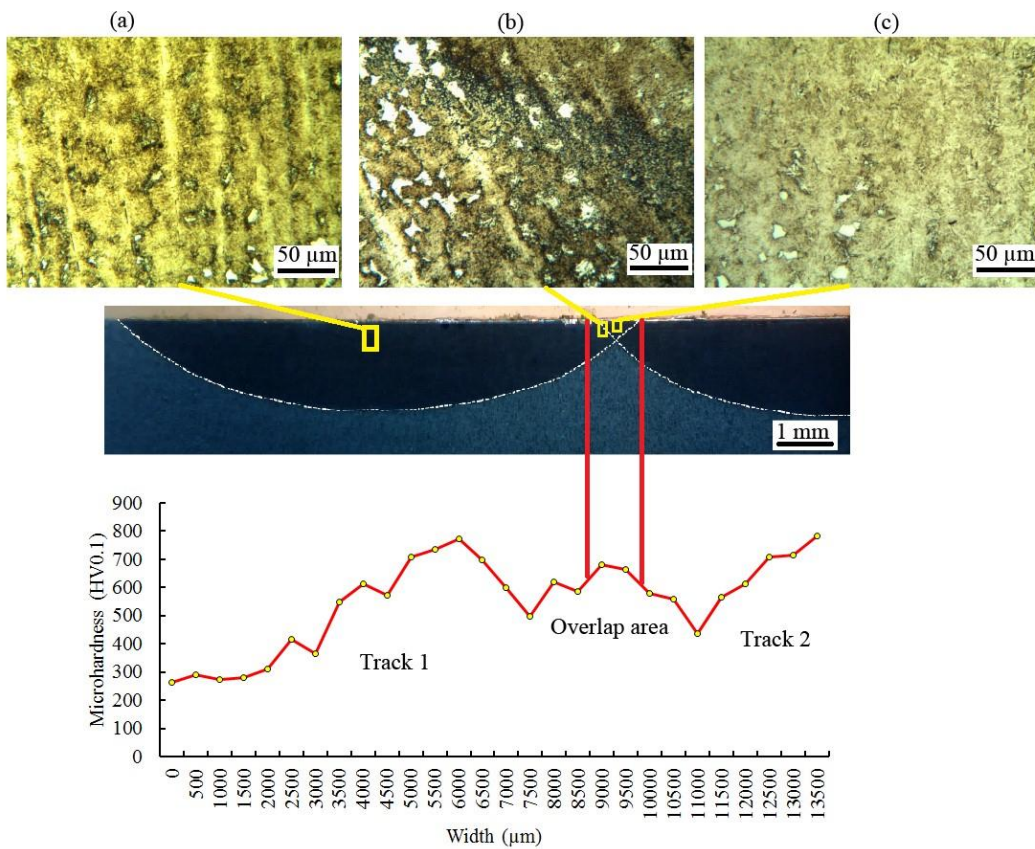


Figure 21. 30% Overlap diagram schematic, microstructure and microhardness distribution

## 6. Conclusions

In this study, the effect of the scanning speed, the laser power, and the laser focal plane position are investigated in diode laser surface hardening process of AISI 4130 by using Design of Experiments. According to experimental works, the following results concluded:

1. Results displayed that by decreasing the scanning speed and increasing the laser power the heat input of the laser increases, which lead to increases the geometrical dimensions of the hardened zone and its hardness. Also by reduction in the focal plane position because of increasing the beam density, a better laser hardening process is conducted.
2. By conducting a multi-response optimization, through desire ability approach, the optimum settings of the diode laser surface hardening of AISI 4130 are: scanning speed (S) = 4.45 mm/s, laser power (P) = 1491 W, focal plane position (FPP) = 62 mm, while the beam density is 84 W/mm<sup>2</sup>.
3. In the best optimum condition the hardness of the diode laser hardening process is 3 times of the hardness of the base metal. Increases of microhardness from 265 Hv to 798 HV with depth of 1.310 mm and width of 9.883 mm.
4. By conducting the overlapping tests in 50% and 30% in order to scan the surface in the optimum setting, the hardness of the overlapped area increases comparing with the single track. In the 50% overlapping the hardness distribution is more smooth and uniform than the 30% one.
5. The microstructure could be controlled by controlling the process parameters. Laser surface hardening engineering of carbon steel AISI 4130 causes changing initial phases of the base metal to martensitic phase. Results show that having less ferrite percentage in microstructure phases causes more hardness.

## 7. References

- [1] J. W. HILL, M. J. LEE and I. J. SPALDING, Surface treatments by laser, OPTICS AND LASER TECHNOLOGY. (1974) 276-278.
- [2] J. BENEDEK, A. SHACHRAI and L. LEVIN, Case hardening of steel by a CO<sub>2</sub>, laser beam, OPTICS AND LASER TECHNOLOGY. (1980) 247-253.
- [3] L.J. YANG, S. JANA and S.C. TAM, Laser Transformation hardening of tool steel specimens, Journal of Materials Processing Technology. 21 (1990) 119-130.
- [4] H.J. Shin, Y.T. Yoo, D.G. Ahn and K. Im, Laser surface hardening of S45C medium carbon steel using ND:YAG laser with a continuous wave, Journal of Materials Processing Technology. 187 (2007) 467-470.
- [5] Flavia Aline Goia and Milton Sergio Fernandes de Lima, Surface Hardening of an AISI D6 Cold Work Steel Using a Fiber Laser, Journal of ASTM International. 8 (2010) 1-9.
- [6] D. Babu.P, G.Buvanashakaran, Experimental studies on the microstructure and hardness of laser transformation hardening of low alloy steel, Transactions of the Canadian Society for Mechanical Engineering. 36 (2012) 241-258.

- [7] Adel K. M, Enhancement of Dry Sliding Wear Characteristics of CK45 Steel Alloy by Laser Surface Hardening Processing, *Procedia Materials Science*. 6 (2014) 1639 – 1643.
- [8] Peipei Sun, Shaoxia Li, Gang Yu, Xiuli He, Caiyun Zheng and Weijian Ning, Laser surface hardening of 42CrMo cast steel for obtaining a wide and uniform hardened layer by shaped beams, *Int J Adv Manuf Technol*. 70 (2014) 787–796.
- [9] R .Li, Y. Jin, Z. Li, K. Qi, A Comparative Study of High-Power Diode Laser and CO2 Laser Surface Hardening of AISI 1045 Steel, *Journal of Materials Engineering and Performance*. 23 (2014) 3085-3091.
- [10] I. A. Pinahin, V. A. Chernigovskij, A. A. Bracihin, and M. A. Yagmurov,,” Improvement of Wear Resistance of VK6, VK8, T5K10 and T15K6 Hard Alloys by Volume Pulsed Laser Hardening, *Friction and wear*.36 (2015) 330-333.
- [11] A. V. Aborkin, V. E. Vaganov, A. N. Shlegel and I. M. Bukarev, Effect of laser hardening on die steel microhardness and surface quality, *Metallurgist*. 59 (2015) 619-625.
- [12] Anna Bień, Marek Szkodo, Surface treatment of C80U steel by long CO2 laser pulses, *Journal of Materials Processing Technology*. 217 (2015) 114–121.
- [13] G. Telasang, J. DuttaMajumdar, G. Padmanabham, I.Manna,Wear and corrosion behavior of laser surface engineered AISI H13 hot working tool steel, *Surface & coatings technology*. 261 (2015) 69-78.
- [14] F. Cordovilla, A. G. Beltra, P. Sancho, J. Domínguez, L. R. de Lara, J. Ocaña, Numerical/experimental analysis of the laser surface hardening with overlapped tracks to design the configuration of the process for Cr-Mo steels, *Materials & Design*. 102 (2016) 225-237
- [15] S. Guarino, M. Barletta and Abdelkarim Afilal, High Power Diode Laser (HPDL) surface hardening of low carbonsteel: Fatigue life improvement analysis, *Journal of Manufacturing Processes*. 28 (2017) 266–271.
- [16] M Moradi, MM Fallah, S Jamshidi Nasab. Experimental Study of Surface Hardening of AISI 420 Martensitic Stainless Steel Using High Power Diode Laser. *Transactions of the Indian Institute of Metals*. 71 (2018) 243-250.
- [17] D. S. Badkar, K. S. Pandey, G. Buvanashakaran, Effects of laser phase transformation hardening parameters on heat input and hardened-bead profile quality of unalloyed titanium, *Transactions of nonferrous Metals Society of China*. 20 (2010) 1078-1091.
- [18] Montgomery DC. *Design and analysis of experiments*. New York: John Wiley; (2009).
- [19] Myers RH, Montgomery DC. *Response surface methodology: process and product optimization using designed experiments*. New York: Wiley; (1995).
- [20] Yuchao Bai, Yongqiang Yang, Zefeng Xiao, Mingkang Zhang, Di, Wang, Process optimization and mechanical property evolution of AlSiMg0.75 by selective laser melting, *Materials & Design*. 140 (2018) 257-266.
- [21] M Moradi, E Golchin, Investigation on the Effects of Process Parameters on Laser Percussion Drilling Using Finite Element Methodology; Statistical Modelling and Optimization.. *Latin American Journal of Solids and Structures*. 14 (2017) 464-484.
- [22] M Moradi, AR Mohazabpak, Statistical Modelling and Optimization of Laser Percussion Microdrilling of Inconel 718 Sheet Using Response Surface Methodology (RSM), *Lasers in Engineering*. 39 (2018) 313-331.
- [23] M Moradi, O Mehrabi, T Azdast, KY Benyounis, Enhancement of low power CO2 laser cutting process for injection molded polycarbonate. *Optics & Laser Technology*. 96 (2017) 208–218.

- [24] Elijah Kannatey Asibu Jr. Principles of Laser Material Processing, New Jersey: Published by John; (2009).
- [25] George F. Vander Voort, ASM Handbook Volume 9: Metallography and Microstructures, the materials information company (1992).
- [26] Mahmoud Moradi, Reza AbbasiRad, Majid Ghoreishi, Hadi Abdollahi, Majid Rostami, Investigation and Optimization of EDM Milling and its Comparison with Die Sink EDM, International Journal of Advanced Design and Manufacturing Technology (ADMT). 10 (2017) 33-42.
- [27] Harry chandler, Heat Treater's Guide, Practices and procedures for nonferrous alloys, the materials information company; (1996).